Robust Seasonality of Arctic Warming Processes in Two Different Versions of the MIROC GCM

MASAKAZU YOSHIMORI

Atmosphere and Ocean Research Institute, University of Tokyo, Kashiwa, Japan

AYAKO ABE-OUCHI

Atmosphere and Ocean Research Institute, University of Tokyo, Kashiwa, and Research Institute for Global Change, Japan Agency for Marine-Earth Science and Technology, Yokohama, Japan

MASAHIRO WATANABE AND AKIRA OKA

Atmosphere and Ocean Research Institute, University of Tokyo, Kashiwa, Japan

TOMOO OGURA

National Institute for Environmental Studies, Tsukuba, Japan

(Manuscript received 27 January 2014, in final form 16 May 2014)

ABSTRACT

It is one of the most robust projected responses of climate models to the increase of atmospheric CO_2 concentration that the Arctic experiences a rapid warming with a magnitude larger than the rest of the world. While many processes are proposed as important, the relative contribution of individual processes to the Arctic warming is not often investigated systematically. Feedbacks are quantified in two different versions of an atmosphere–ocean GCM under idealized transient experiments based on an energy balance analysis that extends from the surface to the top of the atmosphere. The emphasis is placed on the largest warming from late autumn to early winter (October–December) and the difference from other seasons. It is confirmed that dominating processes vary with season. In autumn, the largest contribution to the Arctic surface warming is made by a reduction of ocean heat storage and cloud radiative feedback. In the annual mean, on the other hand, it is the albedo feedback that contributes the most, with increasing ocean heat uptake to the deeper layers working as a negative feedback. While the qualitative results are robust between the two models, they differ quantitatively, indicating the need for further constraint on each process. Ocean heat uptake, lower tropospheric stability, and low-level cloud response probably require special attention.

1. Introduction

The Arctic has been experiencing a rapid warming in recent years with magnitude larger than the rest of the world. This so-called Arctic amplification was predicted decades ago by numerical models (Manabe and Wetherald 1975) and verified by observations more recently (Screen and Simmonds 2010a; Serreze et al. 2009). While albedo feedback is the most cited key process, many other processes (e.g., poleward heat transport and cloud changes) operate simultaneously and were also suggested as important in previous studies [as listed in the introduction of Yoshimori et al. (2014, hereafter Y14)]. Quantifying the relative importance of individual effects is one of the essential steps toward an understanding of the underlying mechanisms.

Climate models are built on physical laws and well-designed parameterizations, but how they interact with each other is not always well understood. Once the contribution of individual processes to the Arctic warming is evaluated, more rigorous verification of climate models (e.g., whether or not models reproduce observed warming for the correct reasons) would become possible.

Corresponding author address: Masakazu Yoshimori, Faculty of Environmental Earth Science, Hokkaido University, Kita 10, Nishi 5, Kita-ku, Sapporo 060-0810, Japan.
E-mail: myoshimo@ees.hokudai.ac.jp

DOI: 10.1175/JCLI-D-14-00086.1

The individual contribution to the warming is often evaluated based on the energy balance analysis at the surface or at the top of the atmosphere (TOA) (Kay et al. 2012; Laîné et al. 2009; Ohmura 1984; Taylor et al. 2011a,b; Yoshimori et al. 2009). This approach is particularly useful for multimodel analysis in which available data are limited and additional experiments may not be coordinated easily (Crook et al. 2011; Lu and Cai 2009a). It was shown that the effect of longwave radiation associated with the change in atmospheric temperature profile is one of the dominant terms in the Arctic (Yoshimori et al. 2009). The physical interpretation of this term is, however, unclear because the atmospheric temperature change itself results from a combination of other processes as elaborated by Cai and Lu (2009). Condensation heating or horizontal heat transport, for example, modifies the atmospheric temperature profile, which in turn alters downward longwave radiation to the surface.

Lu and Cai (2009b) took a step forward by formulating a new climate feedback–response analysis method (CFRAM) in which the energy balance analysis is conducted at all levels from the surface to the TOA. The contribution of each process is evaluated taking both air and surface temperature changes into account simultaneously; that is, the remote effect of air temperature change on the surface temperature change through longwave radiation, or vice versa, is included. Lu and Cai (2010) applied this method to an idealized GCM without the hydrological cycle, and Taylor et al. (2013) and Y14 applied it to more complete GCMs. In Y14, for example, 2 and 4 times CO_2 equilibrium experiments of a coupled atmosphere–ocean GCM were analyzed. The diagnosis quantified the relative importance of individual feedbacks and provided insight into what processes contribute to the enhanced Arctic warming with respect to the global average and what processes contribute to the enhanced Arctic surface warming than aloft. Only annual mean CFRAM analysis was carried out in these studies, however. This is a concern as the different physical processes may be dominant in different seasons.

The importance of seasonal heat exchange between the ocean and the atmosphere in simulating the enhanced autumn–winter Arctic warming was pointed out decades ago by Manabe and Stouffer (1980), whose work shows a stark contrast to the strong summer warming induced by albedo feedback without the ocean in Ramanathan et al. (1979). The CFRAM analysis can quantify the relative importance of such a seasonal process among others. In the current study, monthly mean analysis is carried out by taking seasonal ocean heat uptake process into account. We use two different versions of the GCM that significantly differ in atmospheric physics parameterization, aiming to capture the robust response rather than to investigate the difference. The goal of the current study is to reveal how that ''robust'' response may vary with seasons.

The paper is organized as follows. In the next section, the models and experiments are described. The analysis method is explained in section 3. Section 4 presents the results in which an overview of the Arctic near-surface response, performance of the CFRAM analysis, relative contribution of individual processes to Arctic surface warming, role of the ocean heat uptake, and relative contribution of individual processes to Arctic atmospheric temperature profile are given in each subsection. They are followed by a summary subsection that highlights comparisons between the season of strongest warming and the annual mean, and between Arctic and global means. Discussion and conclusions are given in sections 5 and 6, respectively.

2. Models and experiments

The models used in the current study are two different versions of an atmosphere–ocean general circulation model, the Model for Interdisciplinary Research on Climate (MIROC), version 4, medium resolution (MIROC4m) and MIROC version 5 (MIROC5). MIROC4m is essentially the same as the MIROC version 3.2. medium resolution [MIROC3.2(medres); Hasumi and Emori 2004], with which a suite of experiments were archived in phase 3 of the Coupled Model Intercomparison Project (CMIP3; Meehl et al. 2007). MIROC4m was renamed from MIROC3.2(medres) after a bug fix in the surface flux calculation over ice sheets (Chan et al. 2011), but the climatic impact of the fix is minor except for paleoclimate experiments with large ice sheets. A suite of experiments with MIROC5 were archived in phase 5 of CMIP (CMIP5; Taylor et al. 2012).

MIROC4m and MIROC5 atmospheres have horizontal resolutions with spectral truncation T42 (~2.8°) and T85 (~1.4°), and 20 and 40 vertical levels, respectively. Ocean components in MIROC4m and MIROC5 have similar horizontal resolutions of 0.5°–1.4° (numerical poles are shifted from the geographical poles in MIROC5), and 43 and 49 vertical levels (plus 1 bottom boundary layer), respectively. Land surface and sea ice components share the same horizontal resolutions with paired atmosphere and ocean components, respectively, in both models. The major difference between the two models resides in physics parameterizations of the atmosphere (Table 1) and was described by Watanabe et al. (2010) in detail along with their performance. In

TABLE 1. Major differences in MIROC4m and MIROC5 physics representation modified from Table 1 of Watanabe et al. (2012) [see Watanabe et al. (2010) and Komuro et al. (2012) for details].

Component	Physics	MIROC4m	MIROC5
Atmosphere	Cumulus convection	Prognostic Arakawa–Schubert (AS) scheme with a triggering function	Prognostic AS with state-dependent entrainment
	Large-scale condensation and microphysics	Diagnostic cloud fraction with temperature-dependent water–ice partition	Prognostic probability density function (PDF) for cloud fraction with mixed-phase microphysics
	Turbulence	Level 2.0 closure	Level 2.5 closure
Sea ice	Thickness representation	Two categories	Thickness distribution

the context of climate sensitivity, a gap in physical parameterization between the two models was also investigated by replacing key parameterizations in one model individually or in combination by those in the other model (Shiogama et al. 2014; Watanabe et al. 2012). Despite the considerable difference in formulations of the two models, there are many common features in Arctic warming processes that are investigated in this article.

We analyze the results of two experiments for each model: a preindustrial control simulation and an annually increasing CO_2 experiment (1% increase from the previous year, 1pctCO2), starting from the control simulation. In the 1pctCO2 experiment, CO_2 concentration reaches twice the level of initial concentration at 70 years, and the 20-yr average from years 61 to 80 is used for the analysis. Three members were generated for MIROC4m in which each ensemble member differs in its initial state: they are taken from the control with at least 40 years apart from each other. Only a single run was made for MIROC5 because of limited available computational resources. The control simulations were continued from the same initial conditions in parallel to 1pctCO2, and the corresponding years were subtracted from 1pctCO2 to obtain the response to CO_2 increase.

3. Analysis method

Our analysis is based on energy budget of the atmosphere and ocean. For the quantification of relative contribution of individual processes to the simulated temperature change, the CFRAM developed by Lu and Cai (2009b) is applied. This is mathematically an extension of the surface energy balance analysis used in Ohmura (1984), Laîné et al. (2009), and Lu and Cai (2009a) to the entire atmosphere-surface column, but the CFRAM analysis implicitly includes the TOA energy balance analysis that is not included in the surface analysis (the vertical integration of the CFRAM energy balance equations leads to the TOA energy balance equation).

We begin with the conventional perturbed surface energy balance equation written as

$$\Delta R_{\mathrm{LW}\uparrow} = \Delta R_{\mathrm{SW}} + \Delta R_{\mathrm{LW}\downarrow} + \Delta Q \tag{1}$$

and

$$\Delta Q \equiv \Delta H - L\Delta E - \Delta G - \Delta M, \tag{2}$$

where R_{SW} and R_{LW} are net downward shortwave radiation and longwave radiation ($\uparrow$ for upward, and $\downarrow$ for downward), respectively, with the perturbation denoted by Δ. Also, H, E, and L are sensible heat flux (downward taken as positive), evaporation, and latent heat of vaporization, respectively; G represents heat transported into the subsurface while M is latent heat consumed for melting of snow and ice. Approximating the surface emissivity to one, the surface temperature T_S is expressed by the sum of individual energy flux terms:

$$\Delta T_S = (4\sigma T_S^3)^{-1}(\Delta R_{\mathrm{SW}} + \Delta R_{\mathrm{LW}\downarrow}^{\mathrm{EXT}} + \Delta R_{\mathrm{LW}\downarrow}^{\mathrm{WVP}} + \Delta R_{\mathrm{LW}\downarrow}^{\mathrm{CLD}} + \Delta R_{\mathrm{LW}\downarrow}^{T} + \Delta Q), \tag{3}$$

where σ is the Stefan–Boltzmann constant. The downward longwave radiation here consists of external forcing (EXT), water vapor (WVP), cloud (CLD), and temperature (T) components. Naturally, $\Delta R_{\mathrm{LW}\downarrow}^{T}$ results from all processes that alter air temperature. By using the CFRAM, this term is further decomposed into individual processes as in the following.

The perturbed energy balance equation for the entire atmosphere–surface column in the CFRAM is written as

$$\Delta \mathbf{T} = \left(\frac{\partial \mathbf{R}_{\mathrm{LW}}}{\partial \mathbf{T}}\right)^{-1}(\Delta \mathbf{R}_{\mathrm{SW}} + \Delta \mathbf{R}_{\mathrm{LW}}^{\mathrm{EXT}} + \Delta \mathbf{R}_{\mathrm{LW}}^{\mathrm{WVP}} + \Delta \mathbf{R}_{\mathrm{LW}}^{\mathrm{CLD}} + \Delta \mathbf{Q}), \tag{4}$$

$$\Delta \mathbf{R}_{\mathrm{SW}} \equiv \Delta \mathbf{R}_{\mathrm{SW}}^{\mathrm{EXT}} + \Delta \mathbf{R}_{\mathrm{SW}}^{\mathrm{WVP}} + \Delta \mathbf{R}_{\mathrm{SW}}^{\mathrm{ALB}} + \Delta \mathbf{R}_{\mathrm{SW}}^{\mathrm{CLD}}, \tag{5}$$

and

TABLE 2. A list of abbreviations used for individual partial temperature change terms diagnosed using the CFRAM technique.

Category	Abbreviation	Description
Radiative	EXT	External forcing (2 × preindustrial CO_2)
	WVP	Water vapor
	ALB	Surface albedo
	CLD	Clouds
Nonradiative	EVP	Latent heat flux due to surface evaporation
	SH	Surface sensible heat flux
	LSC	Large-scale condensation
	CUM	Cumulus convection
	VDF	Boundary layer process (vertical diffusion)
	DYN	Dynamical heating (including advection, expansion, and contraction of air parcels)
	RESA	Atmospheric heat storage (plus heating due to dry adjustments for MIROC4m)
	RESS	Net surface energy flux (obtained as a residual of net radiation, latent heat flux associated with evaporation, and sensible heat flux)
	RES	Residual term (RESA + RESS)
Others	ALL	Sum of all CFRAM partial temperature changes
	SIM	Simulated (non-CFRAM) temperature change

$$\Delta\mathbf{Q} \equiv \Delta\mathbf{Q}^{\mathrm{EVP}} + \Delta\mathbf{Q}^{\mathrm{SH}} + \Delta\mathbf{Q}^{\mathrm{LSC}} + \Delta\mathbf{Q}^{\mathrm{CUM}} + \Delta\mathbf{Q}^{\mathrm{VDF}} + \Delta\mathbf{Q}^{\mathrm{RES}}, \quad (6)$$

where $\mathbf{T} = (T_1, T_2, \ldots, T_N, T_S)^{\mathrm{T}}$ is a transposed vector of temperature at N atmospheric levels and a surface (T_S) level; $\mathbf{R}$ and $\mathbf{Q}$ are vectors of radiative and nonradiative energy flux convergences, respectively, at $N + 1$ different levels in the column. Individual terms and their abbreviations are explained in Table 2. Also, $\partial\mathbf{R}_{\mathrm{LW}}/\partial\mathbf{T}$ is an $(N + 1) \times (N + 1)$ matrix that represents divergence of longwave radiation per unit temperature increase. Note that additivity of individual radiative effects and linearity of ΔR_{LW} with respect to ΔT are assumed in Eq. (4). Its validity is demonstrated in section 4b by comparing the sum of all terms on the right-hand side with the left-hand side obtained from the simulations. Unlike Eq. (3), the right-hand side of Eq. (4) does not contain a longwave radiation term that depends on the atmospheric temperature change ($\Delta R^{T}_{\mathrm{LW}\downarrow}$). In Eq. (4), the term for atmospheric temperature profile change (i.e., lapse-rate feedback if formulated on the right-hand side) appears on the left-hand side, and is explained by other processes on the right-hand side.

Procedure of the analysis essentially follows Y14: Radiative terms in the CFRAM are quantified using the radiative kernel technique (Soden et al. 2008), and nonradiative terms in the CFRAM are either taken from surface energy fluxes or converted from atmospheric heating rate in model output. It differs from Y14, however, in four points. The first difference is that partial temperature change (i.e., each energy flux contribution) in Eq. (4) is evaluated monthly, rather than annually. The second difference is that atmospheric heat storage term (CdT/dt) ignored for the equilibrium annual mean analysis in Y14 is now included in $\Delta\mathbf{Q}^{\mathrm{RES}}$ for the transient and seasonal analysis. Here, C and t are heat capacity of each atmospheric layer and time, respectively. The third difference is that the cloud radiative feedback is calculated by adjusting the cloud radiative effect (CRE) with cloud masking effect on radiative perturbations by noncloud variables (i.e., CO_2, water vapor, temperature, and surface albedo). The CRE is defined as the difference in radiative fluxes between average-sky and clear-sky conditions. This is an extension of the adjusted CRE technique at the top of the atmosphere introduced by Soden et al. (2008) to the entire atmosphere–surface column. In Y14, the cloud feedback was calculated as a residual of the radiative heating term using the simulated temperature change. As the current method does not use simulated temperature change directly, it allows us to evaluate the accuracy of the CFRAM analysis by comparing the total sum of partial temperature changes with simulated temperature change. The fourth difference is that the partial temperature change due to surface albedo is diagnosed by using effective albedo change, rather than albedo change averaged over the analysis period. The effective albedo here means the ratio of monthly mean upward and downward shortwave radiation at the surface, which is different from a monthly mean of albedo at every time step. The overall performance is presented in section 4b.

4. Results

a. Simulated changes near the surface

We begin with an overview of the simulated changes near the surface. Figure 1 shows time series of annual mean surface air temperature changes from the control

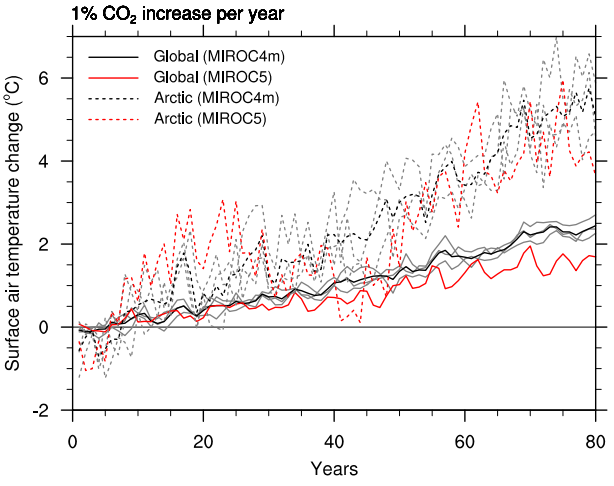

FIG. 1. Time series of annual mean surface air temperature change from the control simulations [global, solid lines and Arctic (70°–90°N), dashed lines]. Gray lines represent individual simulations, and black lines represent the ensemble mean of the three simulations with MIROC4m. MIROC5 (red) has only one member.

simulations averaged over the entire globe or Arctic. We define 70°–90°N as the Arctic throughout this paper. Although this choice is somewhat arbitrary, we find from later analysis that seasonal processes over land (occupying a large part of 60°–70°N) and ocean (occupying a large part of 70°–90°N) are substantially different, and we focus on the latter. The global mean temperature change for MIROC4m becomes gradually larger than MIROC5, consistent with the difference in their climate sensitivity (MIROC4m of 4.0°C and MIROC5 of 2.7°C). The climate sensitivity of MIROC5 is taken from Andrews et al. (2012) and calculated for MIROC4m with the same method, that is, a regression analysis on the initial 150-yr data from an abrupt quadrupling CO_2 experiment. While the MIROC4m Arctic temperature displays approximately a monotonic increase, MIROC5, having a faster rate of Arctic warming during the initial 25 years, exhibits a dip from about 25 to 50 years. This interdecadal dip is unlikely due to internal variability because the amplitude of about 2°C is much larger than that obtained from the 200-yr-long MIROC5 unforced control simulation (standard deviation of 0.56°C). Time series of the Atlantic meridional overturning circulation (AMOC) and a spatial pattern of surface temperature change (not shown) suggest that the dip in MIROC5 is caused by a rapid weakening of the AMOC, which is more gradual in MIROC4m. Continuous global-scale warming and AMOC-induced local cooling result in the apparent intermission of Arctic warming. This result indicates that AMOC weakening may have a significant impact on the speed of the Arctic mean warming.

Hereafter, all presented results are averages of the last 20 years of the experiments, and the ensemble mean for MIROC4m. The largest Arctic warming occurs from late autumn to early winter [October–December (OND)] while the least warming occurs in summer (June and July). In addition, the largest reduction of Northern Hemisphere sea ice cover occurs in between (August and September), characterizing a strong seasonality of Arctic response. Some of the numerical values are summarized in Table 3 and indicate a stronger Arctic amplification in MIROC5 than MIROC4m.

b. CFRAM total temperature changes

Seasonal distributions of simulated zonal mean surface (skin) temperature changes from the control simulations are shown by color shadings in Fig. 2. There is a stark contrast between the two poles: a large warming at the Northern Hemisphere high latitudes and little warming at the Southern Hemisphere high latitudes. It is well known the latter is due to the large effective heat capacity of Southern Ocean that transports anomalous heat into deeper layers and delays appearance of the near-surface warming. The warming in the Arctic appears to start to the north of 70°N in early autumn and then to spread toward 60°N in both models. We focus our analysis on the OND average when the largest warming occurs although the result of other seasons is presented as necessary.

TABLE 3. Summary of surface air temperature response for the years 61–80 (global mean, T_G; Arctic mean, T_A; and difference from control, Δ).

Experiments	Season	T_G (°C)	ΔT_G (°C)	T_A (°C)	ΔT_A (°C)	$\Delta T_A/\Delta T_G$
MIROC4m control	Annual	13.2	—	−15.1	—	—
	OND	12.3	—	−21.9	—	—
MIROC4m 2 × CO_2	Annual	15.3	2.1	−10.3	4.8	2.2
	OND	14.5	2.3	−14.3	7.7	3.4
MIROC5 control	Annual	14.5	—	−16.8	—	—
	OND	13.5	—	−23.6	—	—
MIROC5 2 × CO_2	Annual	16.0	1.5	−12.5	4.3	2.8
	OND	15.2	1.6	−16.1	7.5	4.6

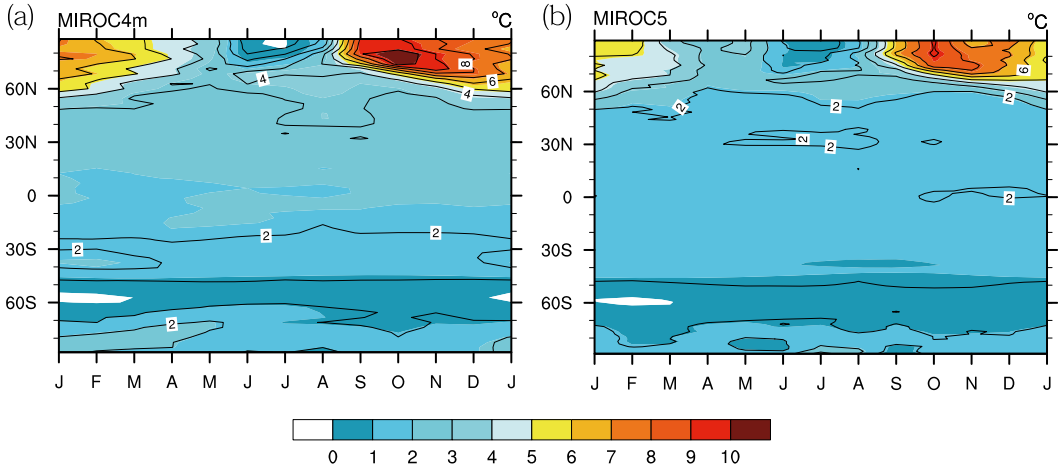

FIG. 2. Changes in zonal mean surface (skin) temperature (°C) from the control simulations for (a) MIROC4m and (b) MIROC5. Color shadings represent simulated temperature change, and line contours represent sum of individual partial temperature changes diagnosed using the CFRAM technique.

Surface and atmospheric temperature changes from the control simulations in OND are shown in color shadings in Fig. 3. At the surface, more than 6°C warming is seen in most of the Arctic Ocean with more than 10°C warming in the Barents Sea, Chukchi Sea, and Canadian Archipelago. These are common for both models, but a warming east of Greenland is stronger in MIROC4m than MIROC5. Atmospheric temperature exhibits a well-known feature of pronounced Arctic near-surface warming. The areas of more than 10°C warming at the surface coincide with the regions of large sea ice reduction in the same OND season (Fig. 4). This suggests that sea ice plays a fundamental role.

Line contours in Figs. 3 and 4 show the sum of partial temperature changes diagnosed individually using the CFRAM technique. The close match between color shadings and line contours in these figures demonstrates the accuracy of the CFRAM formulation and procedures. The accuracy of the CFRAM analysis is improved from Y14 because the seasonal dependence of Planck response operator, $\partial \mathbf{R}_{\mathrm{LW}}/\partial \mathbf{T}$, which is sensitive to the background climate, is taken into account. Additional reason is that the linearity assumption of radiative kernel technique works better for a smaller perturbation of transient $2 \times CO_2$ condition than for a larger perturbation of equilibrium $4 \times CO_2$ condition (Vial et al. 2013). Nevertheless, errors of up to a few degrees are realized in summer Arctic region in Fig. 2. We hypothesize that it results from the radiative effect of simultaneous changes in clouds and albedo being different from the sum of individual effects under strong polar summer insolation. In any case, sufficient accuracy is granted for the rest seasons and hence we conclude that it is reasonable to apply the method for evaluation of OND and annual mean Arctic warming processes.

c. *CFRAM partial surface temperature changes*

Figures 5 and 6 show OND partial surface temperature changes for MIROC4m and MIROC5, respectively, diagnosed using the CFRAM technique. We focus here on common features in both models, rather than detailed differences, in order to grasp essential processes for Arctic warming.

The dominant contribution to the surface warming arises from the net surface energy flux (Figs. 5j and 6j), which is discussed in detail in section 4d. The Planck response—direct thermal radiation response to elevated CO_2 (Figs. 5a and 6a)—and water vapor feedback (Figs. 5b and 6b) exhibit relatively homogeneous and moderate warming of 1°–2°C. This occurs throughout a year. Surface albedo feedback has positive values where sea ice cover is reduced (Figs. 5c and 6c), but the magnitude is much smaller than in June–September (not shown) because of little insolation during OND. Cloud feedback shows warming in the majority of the Arctic Ocean (Figs. 5d and 6d) with local enhancement over the reduced sea ice cover (Fig. 4). This occurs through the longwave radiation (i.e., greenhouse effect) and is accompanied by an increase in low-level clouds in both liquid and solid phases (Fig. 7). This cloud feedback persists in the individual months of OND and is common in both models, but the cloud feedback in other months differs between models. In September, for example, low-level cloud increase is common in both models but the sign of net effect resulting from a cancellation between shortwave and longwave radiation differs in the two models.

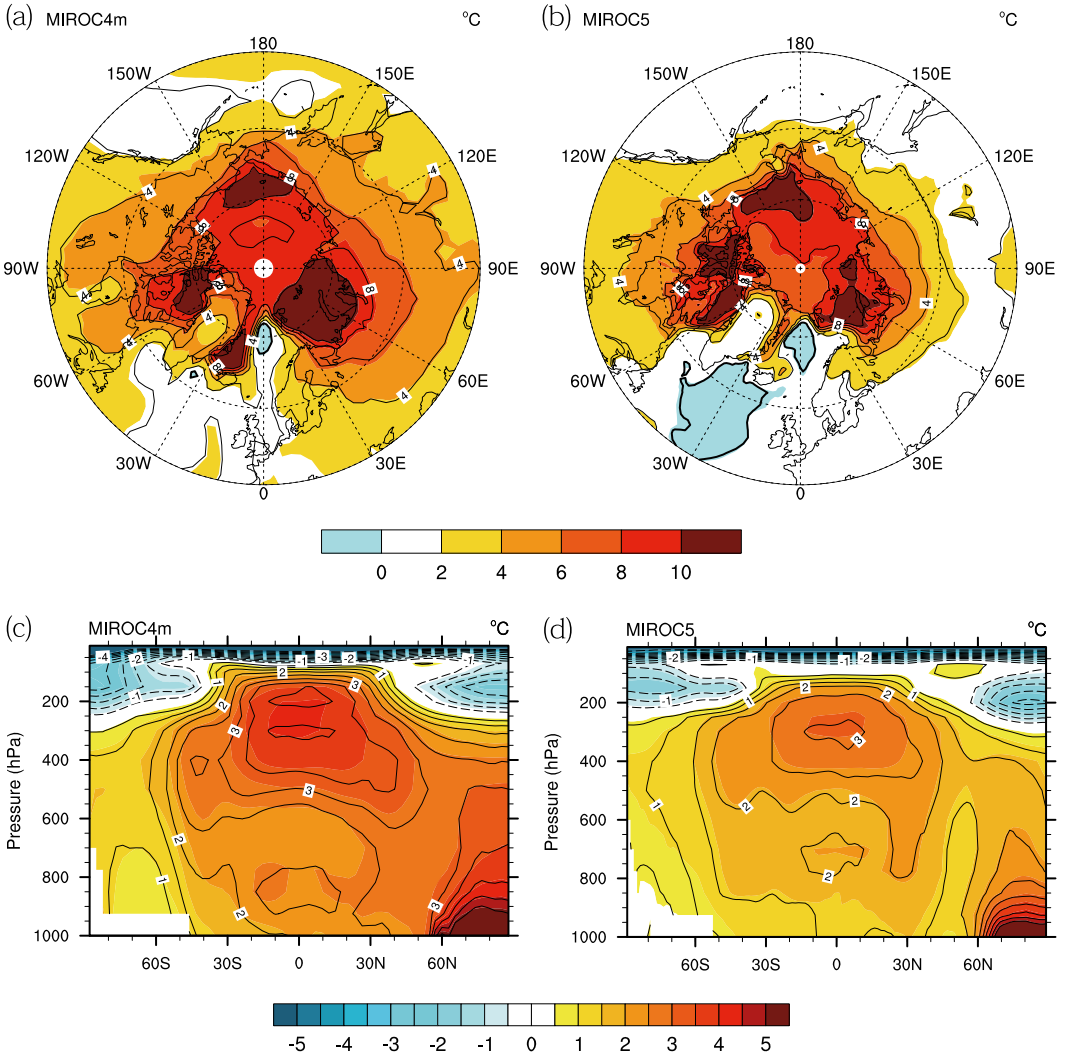

FIG. 3. Temperature changes (°C) from the control simulations averaged over OND (a),(b) at the surface and (c),(d) in the zonally averaged atmosphere, for (left) MIROC4m and (right) MIROC5. Color shadings represent simulated temperature change, and line contours represent sum of individual partial temperature changes diagnosed using the CFRAM technique.

Increased evaporation from the open ocean after sea ice melting has a negative partial temperature change (Figs. 5e and 6e). This evaporative cooling is partially countered by the positive partial temperature change because of increased large-scale condensation with a subsequent increase of downward longwave radiation to the surface (Figs. 5g and 6g). There are locally positive but minor contributions by cumulus convection. The effect of large-scale condensation heating, on the other hand, covers large areas of the Arctic. While moisture is also supplied by surface evaporation (64% and 68% of OND precipitation increase are supplied by surface evaporation in MIROC4m and MIROC5, respectively), it is consistent with the increased poleward transport of latent heat (not shown). Partial temperature change through sensible heat flux (Figs. 5f and 6f) exhibits a similar spatial pattern to evaporative cooling. Both reflect the stability of the near-surface atmosphere. In this season, more warming occurs at the surface than overlying air where sea ice retreats and consequently the stability weakens. In the Norwegian Sea, on the contrary, more warming occurs in the atmosphere than at the underlying surface, which is already warm because of ocean current and provides massive heat to the atmosphere in the control simulation. Partial temperature changes resulting from vertical diffusion (Figs. 5h and 6h) show mirror images of those resulting from sensible heat flux. This is because more sensible heat is extracted from the surface and the anomalous heat spreads throughout the boundary layer via the vertical diffusion, and subsequent increase of downward longwave radiation warms

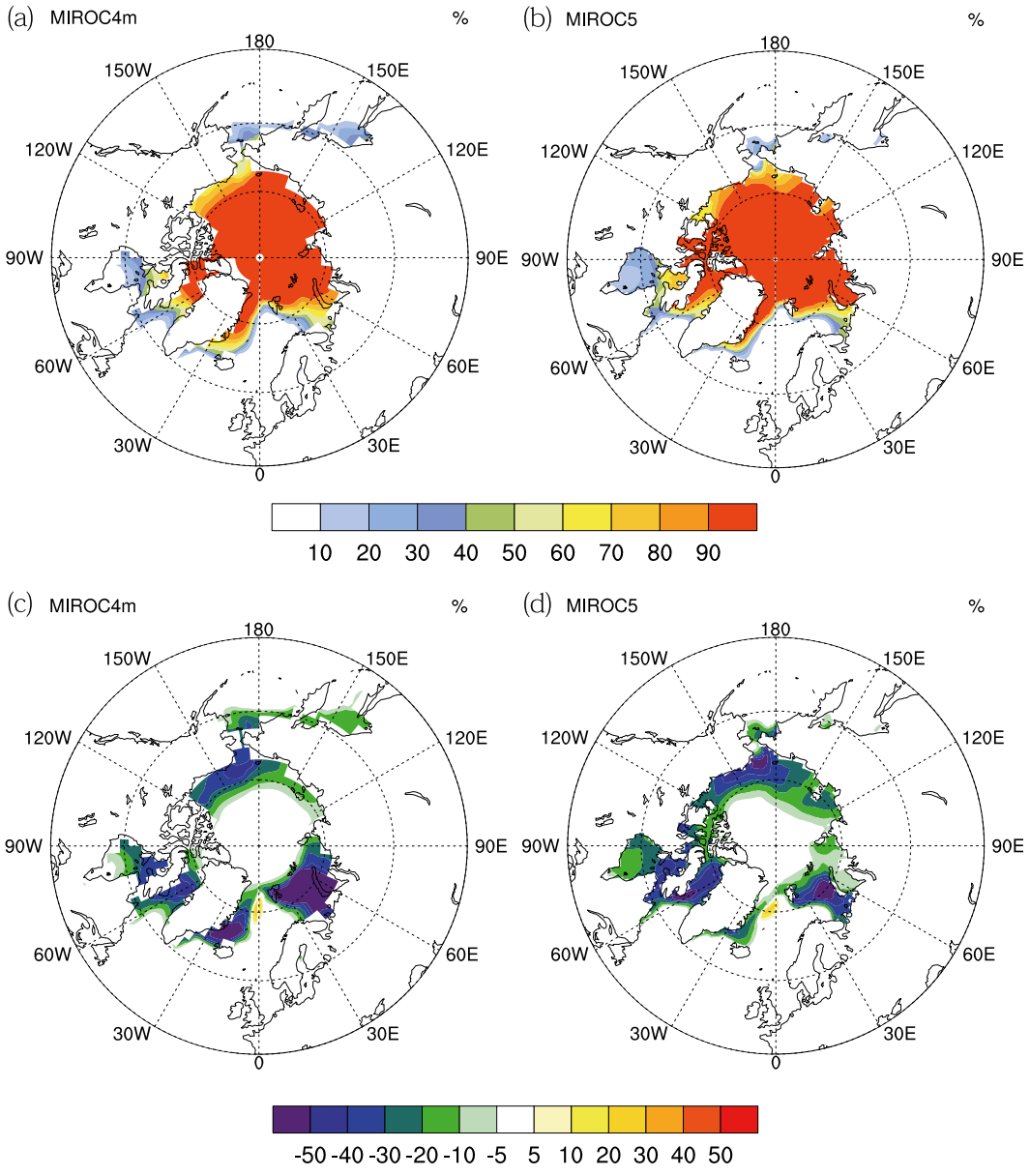

FIG. 4. Sea ice concentration (%) averaged over OND for (a) MIROC4m control, (b) MIROC5 control, (c) MIROC4m 2 × CO_2 change, and (d) MIROC5 2 × CO_2 change.

the surface. It should be noted that heating due to vertical diffusion also includes condensation heating if saturation occurs. It is a matter of concern that the way feedbacks are decomposed into the individual terms in the CFRAM analysis is subject to the convenience of model coding and is somewhat arbitrary.

The spatial pattern of partial temperature change resulting from dynamical heating (Figs. 5i and 6i) is also very similar to that resulting from evaporation and sensible heat flux. We computed the uncentered pattern correlation among the partial surface temperature changes for 70°–90°N (Table 4). Statistical significance is evaluated using the bootstrap resampling method in which paired patterns are randomly ordered for 10 000 times. There are strong correlations (>0.8) among evaporation, sensible heat, vertical diffusion, dynamical heating, and net surface energy flux terms. These spatial patterns correspond to the change in sea ice cover (Figs. 4c,d), indicating the essential effect of sea ice melting on various forms of energy flux.

d. Role of ocean heat uptake in setting seasonality

The net surface energy flux term of the CFRAM analysis (RESS) is obtained as a residual of net radiation,

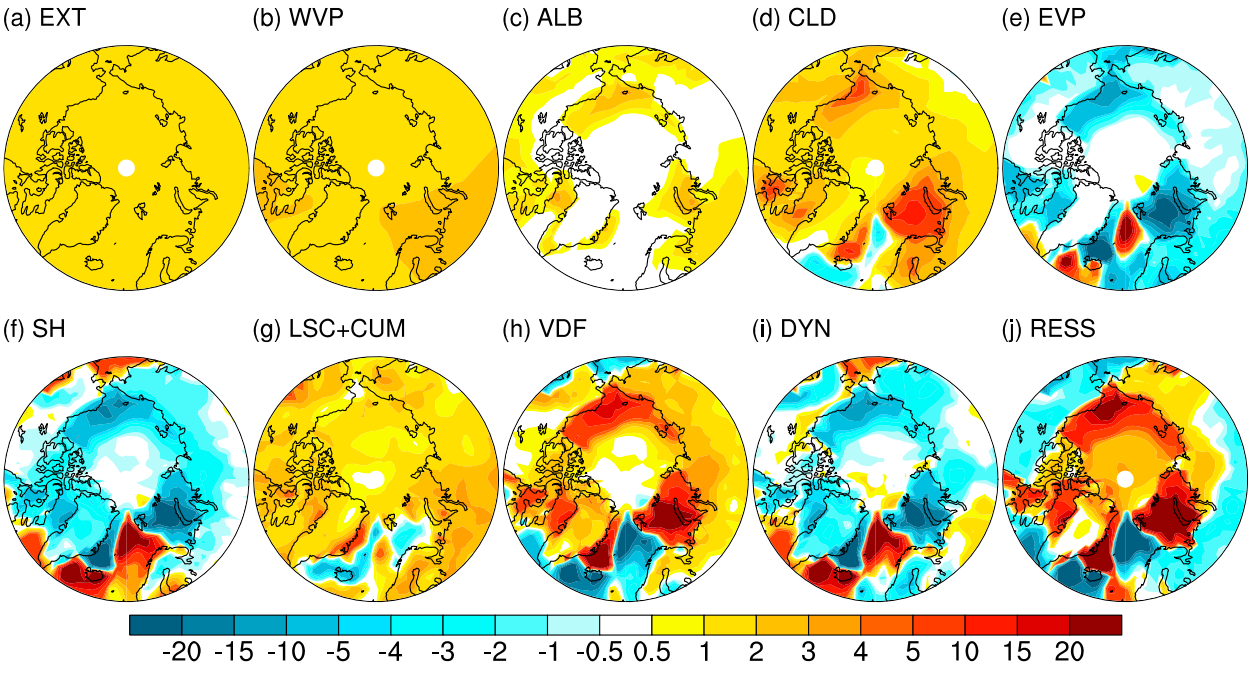

FIG. 5. OND partial surface (skin) temperature changes (°C) in MIROC4m (>60°N) from (a) 2 × CO_2, (b) water vapor, (c) surface albedo, (d) clouds, (e) surface evaporation, (f) surface sensible heat flux, (g) large-scale condensation and cumulus convection, (h) vertical diffusion, (i) dynamical heating, and (j) net surface energy flux. Partial temperature changes due to dry adjustments and atmospheric heat storage are small and not shown.

latent heat flux associated with evaporation, and sensible heat flux. Thus, the RESS term over the Arctic Ocean contains net energy flux into the ocean and latent heat associated with growth and melting of sea ice and snow melting. Figure 8 presents a partition of net surface energy flux into ocean, sea ice, and snow components. The net energy flux into the ocean is obtained directly from the ocean model output. The latent heat associated with

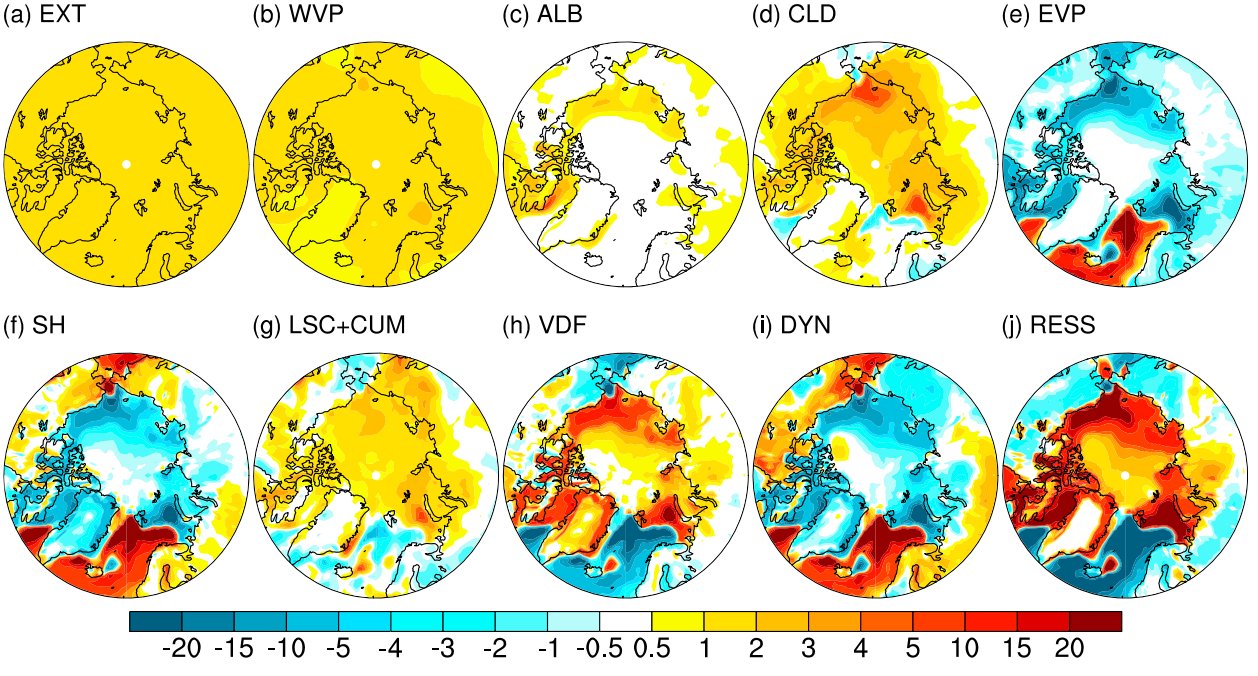

FIG. 6. As in Fig. 5, but for MIROC5. Partial surface temperature change due to atmospheric heat storage is small and not shown.

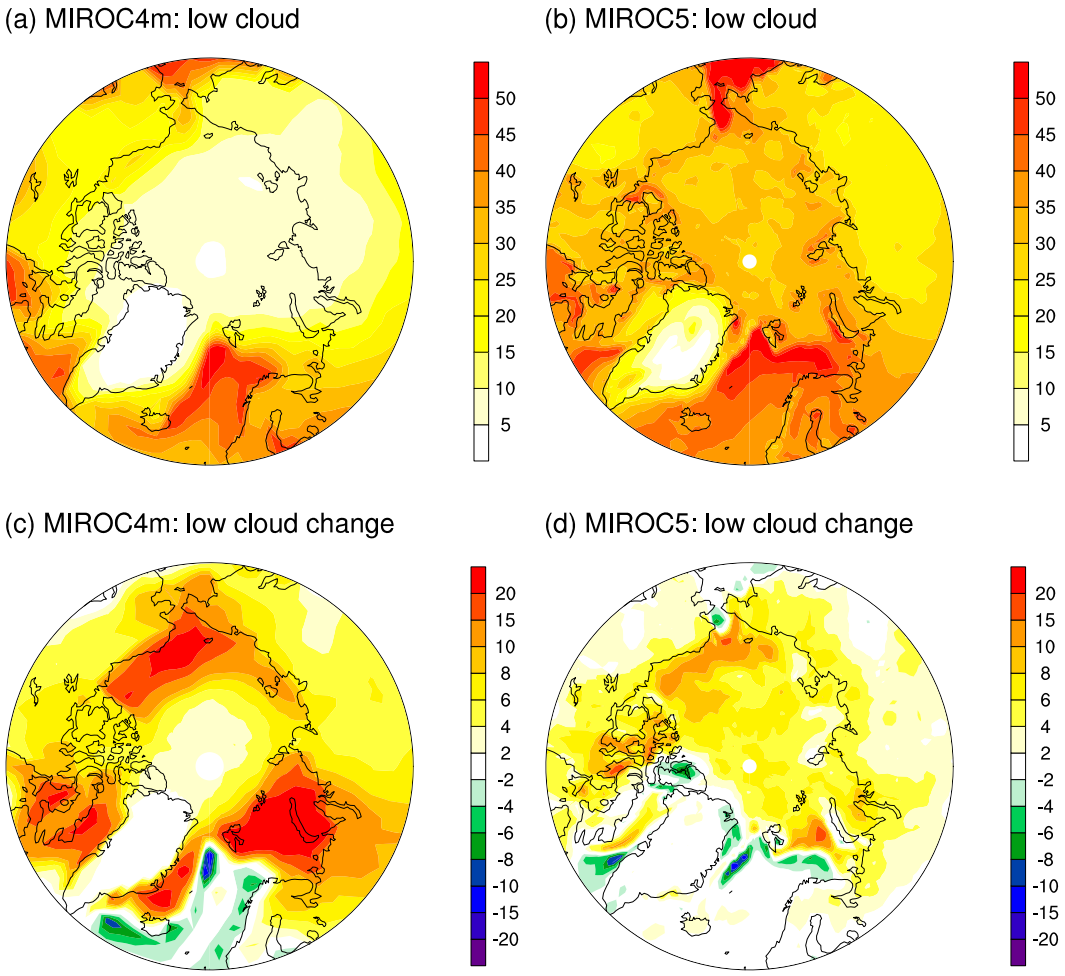

FIG. 7. Low-level cloud amount in OND (%) for (a) MIROC4m control, (b) MIROC5 control, (c) MIROC4m 2 × CO_2 change, and (d) MIROC5 2 × CO_2 change.

growth and melting of sea ice is accurately diagnosed based on the salt budget of sea ice model output. The latent heat used for snow melting is estimated as a residual, which requires interpolation between atmosphere and ocean grids and introduces small errors.

In both models, a dominant energy is used for sea ice melting during summer in the control (Figs. 8a,b). In MIROC4m, smaller amount of sea ice growth under 2 × CO_2 conditions leads to a smaller melting in summer, requiring less heat from the atmosphere to the surface.

TABLE 4. Uncentered pattern correlations among partial surface temperature changes shown in Figs. 5 and 6, for MIROC4m (above the diagonal) and MIROC5 (below the diagonal). Values that are significant at 5% level are presented in boldface. Note, in this table, LSC is the sum of large-scale condensation and cumulus convection.

	EXT	WVP	ALB	CLD	EVP	SH	LSC	VDF	DYN	RESS
EXT	—	0.99	**0.59**	**0.74**	**−0.36**	−0.31	0.66	**0.34**	−0.21	0.30
WVP	**0.98**	—	**0.57**	**0.78**	**−0.40**	−0.32	0.65	**0.36**	−0.22	0.32
ALB	**0.61**	**0.62**	—	**0.62**	**−0.59**	**−0.60**	**0.60**	**0.62**	**−0.52**	**0.56**
CLD	0.79	**0.84**	**0.66**	—	**−0.81**	**−0.59**	0.41	**0.65**	**−0.50**	**0.62**
EVP	**−0.24**	**−0.32**	**−0.48**	**−0.63**	—	**0.87**	**−0.33**	**−0.91**	**0.84**	**−0.91**
SH	−0.11	−0.14	**−0.38**	**−0.53**	**0.83**	—	**−0.53**	**−0.99**	**0.98**	**−0.98**
LSC	0.63	0.67	**0.57**	**0.85**	**−0.72**	**−0.68**	—	**0.53**	**−0.53**	**0.47**
VDF	0.13	0.16	**0.41**	**0.54**	**−0.83**	**−1.00**	**0.70**	—	**−0.97**	**0.98**
DYN	−0.13	**−0.16**	**−0.42**	**−0.54**	**0.86**	**0.99**	**−0.73**	**−0.99**	—	**−0.97**
RESS	0.22	**0.27**	**0.47**	**0.61**	**−0.94**	**−0.96**	**0.75**	**0.96**	**−0.97**	—

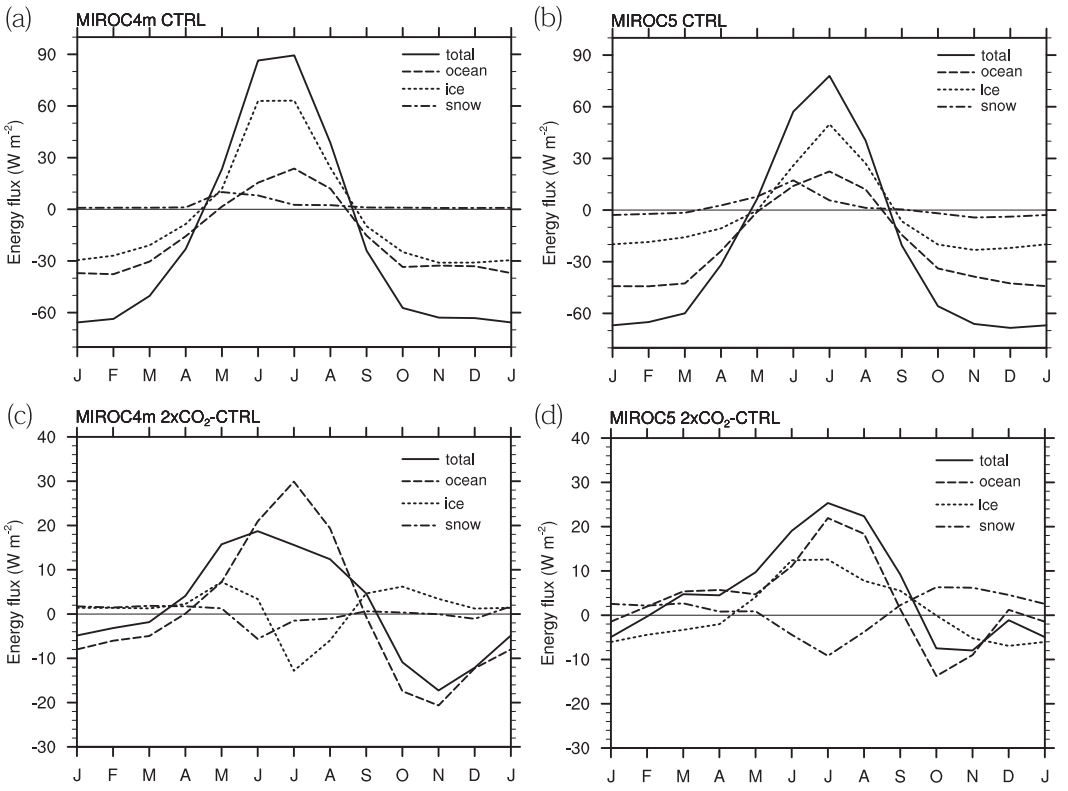

FIG. 8. Seasonal energy exchange in the Arctic Ocean (>70°N) for (a) MIROC4m control, (b) MIROC5 control, (c) MIROC4m 2 × CO_2 change, and (d) MIROC5 2 × CO_2 change. Total (solid lines) is RESS, ocean (dashed lines) is energy flux into the ocean, ice (dotted lines) is latent heat consumed and released with sea ice melting and growth, and snow (dashed-dotted lines) is latent heat consumed for snow melting. Note that the interpolation from atmospheric to ocean grids introduces a small error into the estimate of snow [which must be positive in (a) and (b)].

In MIROC5, on the other hand, larger amount of local sea ice growth in the Greenland Sea leads to a larger melting in summer, requiring more heat from the atmosphere to the surface. Therefore, the change in Arctic latent heat consumption and release associated with sea ice growth and melting tends to have opposite signs between the two models. Nevertheless, RESS in both models varies with season in parallel to the net energy flux into the ocean (Figs. 8c,d).

Figures 9a and 9b show Arctic mean ocean potential temperature changes from the control simulations for MIROC4m and MIROC5, respectively. While magnitude of the ocean warming is substantially different between the two models, there are qualitative similarities: a stronger warming occurs in the upper 50 m from late summer to early autumn and a downward intrusion of temperature anomaly to the depth below 100 m from autumn to winter.

The surface energy flux into the ocean is balanced by the change in Arctic ocean heat content and ocean lateral heat transport. Figure 9c indicates that, in the control experiment, seasonal change in the Arctic Ocean heat storage is controlled by the surface flux rather than the lateral transport, but the annual loss of heat storage through the surface is compensated by relatively constant poleward heat transport. Changes from control experiments under 2 × CO_2 conditions also show that the seasonal change is determined by the surface flux with small influence of the lateral transport (Fig. 9d). As the seasonal distribution of ocean heat uptake is controlled by the mixed layer depth, it is implied that RESS and hence seasonality of Arctic warming is under the strong influence of vertical mixing in the ocean.

Taken together, anomalous heat is absorbed in the ocean during summer and released from the ocean during autumn. The ocean temperature anomaly created during summer causes the strong positive partial temperature change in OND (Figs. 5j and 6j). Although this positive temperature anomaly is counteracted by increased evaporative cooling and extraction of sensible heat, the dominance of the net surface energy flux term in the CFRAM analysis in OND indicates that a significant part of the heat anomaly is emitted in a form of longwave radiation. This is the reason why the Arctic surface warming is strongest in OND.

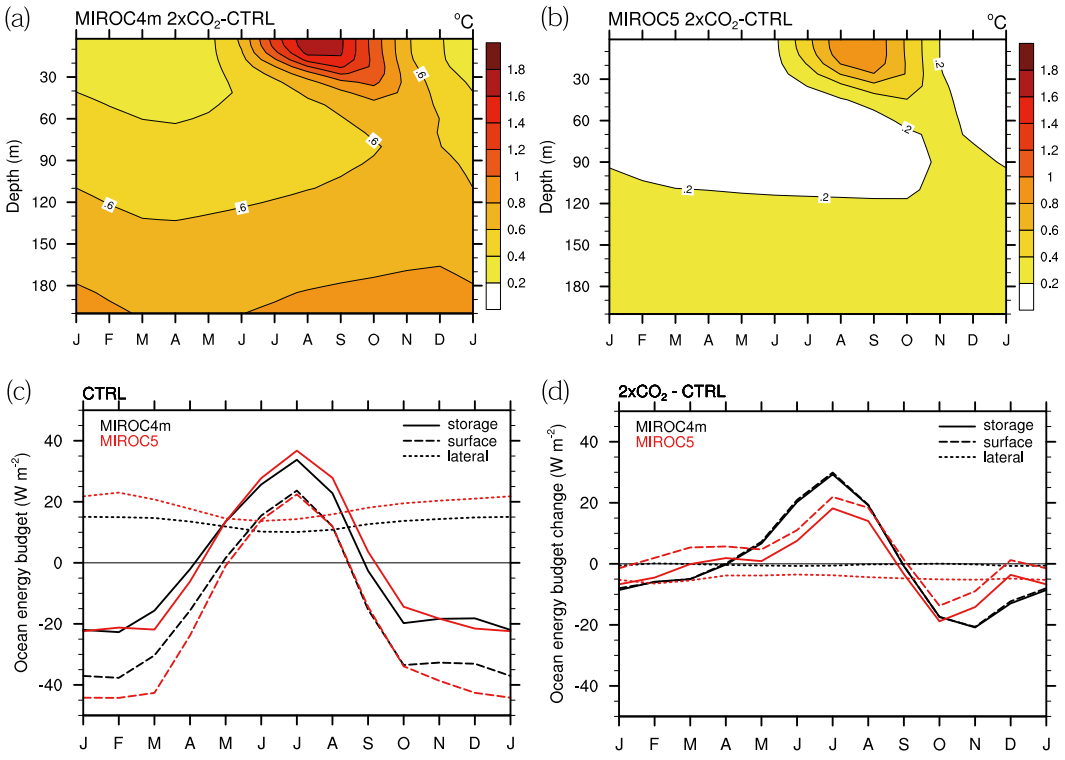

FIG. 9. Seasonal changes in the Arctic Ocean (>70°N) for the top 200-m ocean potential temperature change in (a) MIROC4m and (b) MIROC5. (c) Energy budget and (d) energy budget changes over the full ocean depth from the control simulations. In (c) and (d), positive values indicate net energy gain for the Arctic Ocean.

e. CFRAM partial air temperature changes

There is also a large seasonal variation in processes warming the Arctic atmosphere. Figure 10 shows vertical profiles of atmospheric partial temperature changes in the Arctic for MIROC5. MIROC4m shows a qualitatively similar result as MIROC5 and thus not shown. CO_2 (EXT) and water vapor (WVP) warm the lower troposphere throughout a year. Surface albedo (ALB) shows a very strong near-surface warming in the annual mean, but little in OND. This reflects the strong seasonal variation in Arctic insolation.

In contrast, clouds (CLD) contribute to cooling in the lower troposphere and warming near the surface in OND. At the very near the surface (~1000 hPa), moistening due to increased evaporation occurs but overwhelming warming lowers the relative humidity and reduces the cloud amount. In the lower troposphere (950–800 hPa), on the other hand, the moistening effect overcomes and leads to larger relative humidity and cloud amount. This vertical dipole response coincides with the reduced southward transport of dry-static energy at the very near the surface and the increased northward transport of moisture at relatively higher levels (not shown). The increased cloud amount in the lower troposphere causes a surface warming at the expense of local cooling by increasing the longwave emission. The magnitude of this feedback is probably enhanced by the presence of inversion as the emission depends not only on the emissivity but also on temperature. The warming at the surface and the cooling in the lower troposphere weakens the stability and hence further increases the sensible heat and moisture supply from the surface. Morrison et al. (2012) suggest that this mechanism works as a positive feedback for the cloud formation.

Vertical transport of "moist" energy by surface evaporation (EVP), large-scale condensation (LSC) and cumulus convection (CUM), and of "dry" energy by surface sensible heat flux (SH) and vertical diffusion (VDF) warms the troposphere. The moist energy tends to warm higher levels than the dry energy because the evaporative cooling dominates near the surface and latent heat is "felt" in the atmosphere when the condensation occurs in higher levels. Note that this grouping of moist and dry energy is not very strict as discussed in section 4c. Dynamical heating (DYN) cools the troposphere in both OND and annual means. The magnitude is larger in OND, likely related to a larger reduction of poleward transport of dry-static energy in OND than the annual mean (not shown). DYN only reflects the change in

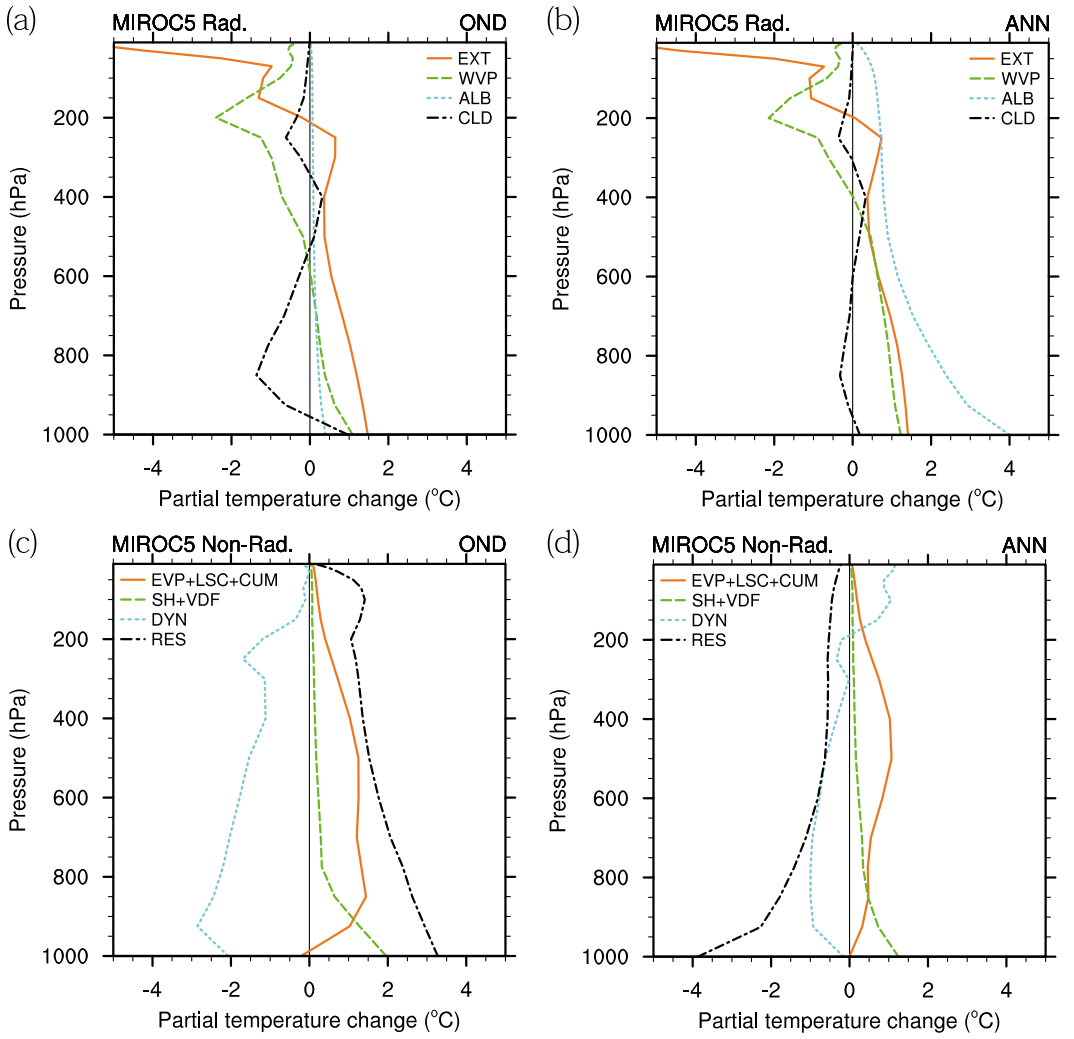

FIG. 10. Vertical profiles of atmospheric partial temperature changes in the Arctic (>70°N) diagnosed using the CFRAM technique for MIROC5 (a) OND and (b) annual mean radiative terms, and (c) OND and (d) annual mean nonradiative terms.

the dry-static energy and not the total moist-static energy, which also includes the moisture component. Ocean processes [from the residual term (RES)] contribute to a strong tropospheric warming in OND by reducing the heat storage so that more energy is emitted from the surface in a form of longwave radiation. In the annual mean, on the contrary, they contribute to a substantial tropospheric cooling as the heat uptake continues during the transient response to the increasing CO_2. Note that the sum of all atmospheric partial temperature profile changes is collectively regarded as a single term, lapse-rate feedback in the conventional radiative feedback analysis at the top of the atmosphere or as a part of downward longwave radiation term in the surface-only energy balance analysis [Eq. (3)].

f. Arctic amplification

Arctic amplification (AA) is referred to an enhanced warming of the Arctic compared to the rest of the world. Here we quantify the contributing processes to the AA by an index (AAI) defined as

$$\mathrm{AAI}_j = (\Delta T_j^{70\mathrm{N}-90\mathrm{N}} - \Delta T_j^{90\mathrm{S}-90\mathrm{N}})/\Delta T_0^{90\mathrm{S}-90\mathrm{N}}, \qquad (7)$$

where ΔT_j denotes the partial temperature change induced by the jth feedback process and ΔT_0 is simulated total temperature change. The superscripts denote the domain of the average. A positive AAI represents the process that maintains an anomalous temperature contrast between the Arctic and the rest of the globe. We evaluate the index at the surface (it was evaluated at the lowest atmospheric level in Y14, but that level differs in

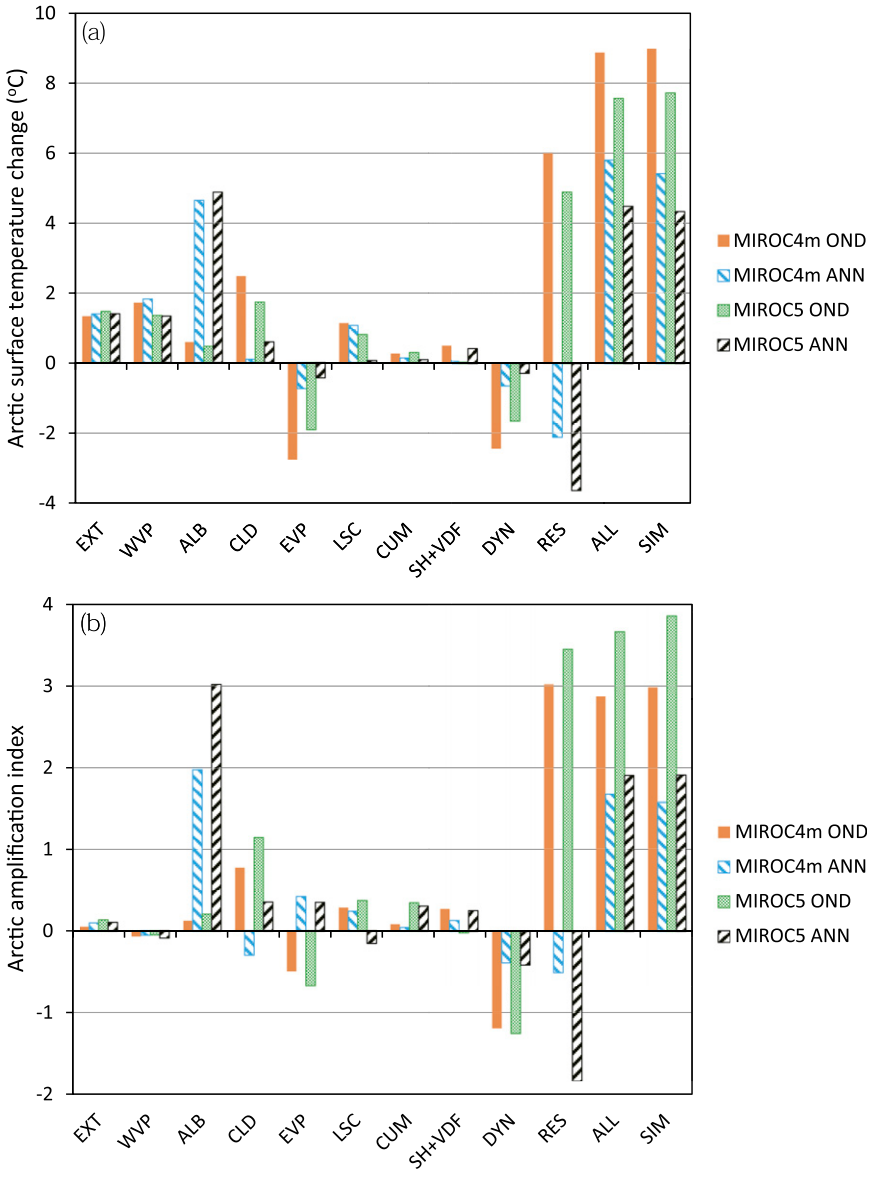

FIG. 11. Partial surface temperature changes diagnosed using the CFRAM technique (EXT–RES), their sum (ALL), and simulated temperature changes (SIM) with (a) Arctic average temperature and (b) AAI. See text for the definition of the AAI. Abbreviations on the bottom are defined in Table 2. The OND and annual (ANN) means for MIROC4m and MIROC5 are shown.

MIROC4m and MIROC5). Figure 11a summarizes the Arctic mean partial surface temperature changes, and Fig. 11b the AAI for OND and annual means. In both Figs. 11a and 11b, simulated changes (SIM) are well reconstructed by the sum of individual partial temperature changes (ALL), supporting the accuracy of the CFRAM analysis.

CO_2 forcing and water vapor feedback contribute positively to the Arctic warming (Fig. 11a), but their magnitude of contribution to the AA (Fig. 11b) is very small (although the CO_2 effect is persistently positive and water vapor effect is persistently negative throughout a year and in the two models). The albedo feedback reveals by far the largest contribution to the Arctic warming and thus to the AA in the annual mean (as shown for the equilibrium cases in Y14), but has little effect during the strongest warming season (OND). The effect of cloud feedback on the Arctic warming is positive in OND, but even the sign of the effect on AA varies with models in the annual mean.

Increased latent heat flux (EVP) from the surface induces Arctic cooling and it is stronger in OND than the annual mean. This evaporative cooling contributes positively to the AA in the annual mean because more evaporation occurs in the lower latitudes as pointed out in Y14. As stated in the previous subsection, the large-scale condensation and cumulus convection have small impact on the surface warming as their influence tend to be more concentrated aloft. Similarly, because of the cancelling nature of the two effects (as discussed in section 4c), surface sensible heat flux plus vertical diffusion (SH + VDF) has little effect on the surface warming. The effect of dynamical heating on Arctic warming is persistently negative and its contribution to the AA is also negative, consistent with Y14. The residual term (RES, mostly representing the ocean heat uptake) exhibits the largest positive contribution to the Arctic warming in OND but negative contribution in the annual mean. Again, this is due to the seasonal reduction of ocean heat storage in OND and continuous heat uptake during the transient response to the increasing CO_2 in the annual mean.

Figure 11b explains the reasons why MIROC5 has stronger Arctic amplification than MIROC4m: a larger albedo feedback in the annual mean and larger cloud feedback and ocean heat storage effect in OND with respect to the global mean. A larger albedo feedback in MIROC5 is, at least partly, due to the higher values assigned to bare ice and fresh snow albedos (Komuro et al. 2012).

5. Discussion

Because of the use of idealized forcing, it is not possible to compare the current result with observations quantitatively. Qualitative comparison is, nevertheless, useful to evaluate the result. Recent observations from satellite and surface indicate an increase of low-level (<2 km) clouds over newly open water during autumn (Eastman and Warren 2010; Kay and Gettelman 2009; Wu and Lee 2012) although other studies largely relying on the 40-yr European Centre for Medium-Range Weather Forecasts (ECMWF) Re-Analysis (ERA-40) and the Interim ECMWF Re-Analysis (ERA-Interim) suggest the opposite (Cuzzone and Vavrus 2011; Schweiger et al. 2008). While the sign of the integrated low-level cloud change is unclear from observations, Palm et al. (2010) confirm the vertical dipole structure of the cloud change in the lower troposphere based on satellite observations, which is consistent with our simulations.

Results obtained in the current study are subject to simplified representation of physical processes in the models. For example, in situ and satellite observations reveal that the surface albedo over sea ice varies during summer by snow metamorphism, snow melting, pond formation, pond drainage, and pond evolution (Perovich et al. 2002; Perovich and Polashenski 2012), but these processes are implicitly and crudely parameterized in the model by setting albedo as a function of temperature.

Results from the current study are also expected to be influenced by model biases. For example, both models overestimate minimum (September) sea ice cover in Barents Sea and maximum (March) sea ice cover in the Kara Sea. This results likely in the overestimation of albedo feedback in these regions (Y14). The spatial correspondence of newly open water and increased surface latent and sensible heat fluxes simulated in the models is consistent with ERA-Interim data (Screen and Simmonds 2010b). MIROC4m and MIROC5, on the other hand, overestimate the inversion strength in OND with respect to the ERA-Interim reanalysis, probably introducing errors into the simulated surface flux change. Both models also overestimate the ocean mixed-layer depth in the Arctic. Annual mean mixed-layer depth based on observational data (Steele et al. 2001) is 35.6 m while that of MIROC4m and MIROC5 is 76.4 and 151.8 m, respectively [the details of this issue are investigated in Komuro (2014)]. A much larger annual range of mixed-layer depth in MIROC5 than MIROC4m may affect the seasonal energy exchange between the atmosphere and ocean, which requires further study. A role of cloud microphysics is also left for future study: more insight may be obtained by combining an ensemble experiment with perturbed cloud microphysics parameters and cloud condensate tendency analysis (Ogura et al. 2008).

There is another school of approach in evaluating feedbacks called the online feedback suppression method (OFSM; Bony et al. 2006). In this approach one or more feedback loops are artificially forced to be turned off (Graversen and Wang 2009; Hall 2004; Hall and Manabe 1999; Schneider et al. 1999; Vavrus 2004). While this approach provides valuable insight into the interaction of the suppressed and nonsuppressed feedbacks, it may force the remaining feedbacks to make up for the suppressed feedback (Hwang et al. 2011). In practice, not all individual contributions are evaluated because of technical hurdles, and there arise many synergy terms, which require an enormous number of experiments and are difficult to interpret (Stein and Alpert 1993). An additional disadvantage is that there are no corresponding observations under the condition of suppressed feedbacks. As the total temperature change derived from the OFSM is different from the partial temperature change derived from the energy balance analysis, the CFRAM

results here are not compared to those OFSM results. We note, however, that it is useful to apply the energy balance (or CFRAM) analysis to the results of the OFSM (Langen et al. 2012).

In relation to the understanding of individual feedbacks, regardless of whether it is obtained from CFRAM or OFSM analysis, more rigorous links of feedbacks to daily or synoptic phenomena are necessary. For example, we need to establish how individual feedbacks such as horizontal heat transport, surface heat flux, and cloud formation and its radiative effect are quantitatively linked with changes in weather regime, storm frequency and path, blocking, off-ice cold air outbreaks, and so on.

6. Conclusions

The seasonality of Arctic warming processes in two versions of MIROC GCM is investigated based on the energy budget analysis. Both models show the strongest surface warming in autumn–winter (OND). The comparison between OND and annual means, both demonstrating sufficient accuracy in the CFRAM analysis, reveals that the dominating processes are very different.

In the annual mean, the contribution of albedo change to the Arctic warming is outstanding, but it is partially countered by ocean heat uptake (more strongly so in MIROC5). The albedo change accounts for the amplified warming in the Arctic compared to the global mean, and it accounts for the stronger Arctic amplification of MIROC5 than MIROC4m. In the OND mean, on the other hand, seasonal reduction of ocean heat storage and increased cloud greenhouse effect contribute to the Arctic warming. The stronger Arctic amplification with respect to the global mean in MIROC5 than MIROC4m in OND is also attributed to these two processes.

Anomalous heat is absorbed in the ocean during summer when insolation is strong and decrease in sea ice and surface albedo is large. It is then released to the atmosphere during autumn–winter. If this release is accomplished by latent heat flux, it results in the surface cooling. If the release is accomplished by sensible heat flux, it warms the lower troposphere through vertical diffusion and has relatively small influence on the surface. A large part of the anomalous heat is, however, emitted by the longwave radiation, which accompanies the surface warming. Putting it differently, the temperature anomaly created in summer stays in the subsurface ocean and reemerges in autumn–winter (when the mixed layer deepens), which increases the emission of longwave radiation from the surface.

These results suggest that ocean heat uptake process, atmospheric stability (which controls surface latent and sensible heat fluxes and other boundary layer processes), and low-level cloud response may require further attention to refine the overall Arctic model response and to better understand the Arctic warming mechanism in the real world.

Acknowledgments. The experiments and analysis were carried out using the JAMSTEC Earth Simulator 2 and NIES supercomputer system (NEC-SX9/A-ECO). We benefitted from discussions with Drs. Yoshiki Komuro, Masato Mori, Manabu Abe, Toru Nozawa, Masato Nozu, and Hideo Shiogama. Constructive comments from two anonymous reviewers are greatly appreciated. We thank the developers of the freely available software NCL. This research was supported by the Environment Research and Technology Development Fund (S-10) of the Japanese Ministry of the Environment, GRENE Arctic Climate Change Research Project, and JSPS KAKENHI Grant 25241005. TO was supported by the Program for Risk Information on Climate Change.

REFERENCES

Andrews, T., J. M. Gregory, M. J. Webb, and K. E. Taylor, 2012: Forcing, feedbacks and climate sensitivity in CMIP5 coupled atmosphere–ocean climate models. *Geophys. Res. Lett.,* **39,** L09712, doi:10.1029/2012GL051607.

Bony, S., and Coauthors, 2006: How well do we understand and evaluate climate change feedback processes? *J. Climate,* **19,** 3445–3482, doi:10.1175/JCLI3819.1.

Cai, M., and J. H. Lu, 2009: A new framework for isolating individual feedback processes in coupled general circulation climate models. Part II: Method demonstrations and comparisons. *Climate Dyn.,* **32,** 887–900, doi:10.1007/s00382-008-0424-4.

Chan, W.-L., A. Abe-Ouchi, and R. Ohgaito, 2011: Simulating the mid-Pliocene climate with the MIROC general circulation model: Experimental design and initial results. *Geosci. Model Dev.,* **4,** 1035–1049, doi:10.5194/gmd-4-1035-2011.

Crook, J. A., P. M. Forster, and N. Stuber, 2011: Spatial patterns of modeled climate feedback and contributions to temperature response and polar amplification. *J. Climate,* **24,** 3575–3592, doi:10.1175/2011JCLI3863.1.

Cuzzone, J., and S. Vavrus, 2011: The relationships between Arctic sea ice and cloud-related variables in the ERA-Interim reanalysis and CCSM3. *Environ. Res. Lett.,* **6,** 014016, doi:10.1088/1748-9326/6/1/014016.

Eastman, R., and S. G. Warren, 2010: Interannual variations of Arctic cloud types in relation to sea ice. *J. Climate,* **23,** 4216–4232, doi:10.1175/2010JCLI3492.1.

Graversen, R. G., and M. H. Wang, 2009: Polar amplification in a coupled climate model with locked albedo. *Climate Dyn.,* **33,** 629–643, doi:10.1007/s00382-009-0535-6.

Hall, A., 2004: The role of surface albedo feedback in climate. *J. Climate,* **17,** 1550–1568, doi:10.1175/1520-0442(2004)017<1550:TROSAF>2.0.CO;2.

——, and S. Manabe, 1999: The role of water vapor feedback in unperturbed climate variability and global warming. *J. Climate,* **12,** 2327–2346, doi:10.1175/1520-0442(1999)012<2327:TROWVF>2.0.CO;2.

Hasumi, H., and S. Emori, Eds., 2004: K-1 coupled GCM (MIROC) description. Center for Climate System Research Tech. Rep., 34 pp.

Hwang, Y.-T., D. M. W. Frierson, and J. E. Kay, 2011: Coupling between Arctic feedbacks and changes in poleward energy transport. *Geophys. Res. Lett.,* **38,** L17704, doi:10.1029/2011GL048546.

Kay, J. E., and A. Gettelman, 2009: Cloud influence on and response to seasonal Arctic sea ice loss. *J. Geophys. Res.,* **114,** D18204, doi:10.1029/2009JD011773.

——, M. M. Holland, C. M. Bitz, E. Blanchard-Wrigglesworth, A. Gettelman, A. Conley, and D. Bailey, 2012: The influence of local feedbacks and northward heat transport on the equilibrium Arctic climate response to increased greenhouse gas forcing. *J. Climate,* **25,** 5433–5450, doi:10.1175/JCLI-D-11-00622.1.

Komuro, Y., 2014: The impact of surface mixing on the Arctic river water distribution and stratification in a global ice–ocean model. *J. Climate,* **27,** 4359–4370, doi:10.1175/JCLI-D-13-00090.1.

——, and Coauthors, 2012: Sea-ice in twentieth-century simulations by new MIROC coupled models: A comparison between models with high resolution and with ice thickness distribution. *J. Meteor. Soc. Japan,* **90A,** 213–232, doi:10.2151/jmsj.2012-A11.

Laîné, A., M. Kageyama, P. Braconnot, and R. Alkama, 2009: Impact of greenhouse gas concentration changes on surface energetics in IPSL-CM4: Regional warming patterns, land–sea warming ratios, and glacial–interglacial differences. *J. Climate,* **22,** 4621–4635, doi:10.1175/2009JCLI2771.1.

Langen, P. L., R. G. Graversen, and T. Mauritsen, 2012: Separation of contributions from radiative feedbacks to polar amplification on an aquaplanet. *J. Climate,* **25,** 3010–3024, doi:10.1175/JCLI-D-11-00246.1.

Lu, J. H., and M. Cai, 2009a: Seasonality of polar surface warming amplification in climate simulations. *Geophys. Res. Lett.,* **36,** L16704, doi:10.1029/2009GL040133.

——, and ——, 2009b: A new framework for isolating individual feedback processes in coupled general circulation climate models. Part I: Formulation. *Climate Dyn.,* **32,** 873–885, doi:10.1007/s00382-008-0425-3.

——, and ——, 2010: Quantifying contributions to polar warming amplification in an idealized coupled general circulation model. *Climate Dyn.,* **34,** 669–687, doi:10.1007/s00382-009-0673-x.

Manabe, S., and R. T. Wetherald, 1975: Effects of doubling CO_2 concentration on climate of a general circulation model. *J. Atmos. Sci.,* **32,** 3–15, doi:10.1175/1520-0469(1975)032<0003:TEODTC>2.0.CO;2.

——, and R. J. Stouffer, 1980: Sensitivity of a global climate model to an increase of CO_2 concentration in the atmosphere. *J. Geophys. Res.,* **85,** 5529–5554, doi:10.1029/JC085iC10p05529.

Meehl, G. A., C. Covey, K. E. Taylor, T. Delworth, R. J. Stouffer, M. Latif, B. McAveney, and J. F. B. Mitchell, 2007: The WCRP CMIP3 multimodel dataset: A new era in climate change research. *Bull. Amer. Meteor. Soc.,* **88,** 1383–1394, doi:10.1175/BAMS-88-9-1383.

Morrison, H., G. de Boer, G. Feingold, J. Harrington, M. D. Shupe, and K. Sulia, 2012: Resilience of persistent Arctic mixed-phase clouds. *Nat. Geosci.,* **5,** 11–17, doi:10.1038/ngeo1332.

Ogura, T., S. Emori, M. J. Webb, Y. Tsushima, T. Yokohata, A. Abe-Ouchi, and M. Kimoto, 2008: Towards understanding cloud response in atmospheric GCMs: The use of tendency diagnostics. *J. Meteor. Soc. Japan,* **86,** 69–79, doi:10.2151/jmsj.86.69.

Ohmura, A., 1984: On the cause of 'Fram' type seasonal change in diurnal amplitude of air temperature in polar regions. *J. Climatol.,* **4,** 325–338, doi:10.1002/joc.3370040309.

Palm, S. P., S. T. Strey, J. Spinhirne, and T. Markus, 2010: Influence of Arctic sea ice extent on polar cloud fraction and vertical structure and implications for regional climate. *J. Geophys. Res.,* **115,** D21209, doi:10.1029/2010JD013900.

Perovich, D. K., and C. Polashenski, 2012: Albedo evolution of seasonal Arctic sea ice. *Geophys. Res. Lett.,* **39,** L08501, doi:10.1029/2012GL051432.

——, T. C. Grenfell, B. Light, and P. V. Hobbs, 2002: Seasonal evolution of the albedo of multiyear Arctic sea ice. *J. Geophys. Res.,* **107,** 8044, doi:10.1029/2000JC000438.

Ramanathan, V., M. S. Lian, and R. D. Cess, 1979: Increased atmospheric CO_2: Zonal and seasonal estimates of the effect on the radiation energy balance and surface temperature. *J. Geophys. Res.,* **84,** 4949–4958, doi:10.1029/JC084iC08p04949.

Schneider, E. K., B. P. Kirtman, and R. S. Lindzen, 1999: Tropospheric water vapor and climate sensitivity. *J. Atmos. Sci.,* **56,** 1649–1658, doi:10.1175/1520-0469(1999)056<1649:TWVACS>2.0.CO;2.

Schweiger, A. J., R. W. Lindsay, S. Vavrus, and J. A. Francis, 2008: Relationships between Arctic sea ice and clouds during autumn. *J. Climate,* **21,** 4799–4810, doi:10.1175/2008JCLI2156.1.

Screen, J. A., and I. Simmonds, 2010a: The central role of diminishing sea ice in recent Arctic temperature amplification. *Nature,* **464,** 1334–1337, doi:10.1038/nature09051.

——, and ——, 2010b: Increasing fall-winter energy loss from the Arctic Ocean and its role in Arctic temperature amplification. *Geophys. Res. Lett.,* **37,** L16707, doi:10.1029/2010GL044136.

Serreze, M. C., A. P. Barrett, J. C. Stroeve, D. N. Kindig, and M. M. Holland, 2009: The emergence of surface-based Arctic amplification. *Cryosphere,* **3,** 11–19, doi:10.5194/tc-3-11-2009.

Shiogama, H., M. Watanabe, T. Ogura, T. Yokohata, and M. Kimoto, 2014: Multi-parameter multi-physics ensemble (MPMPE): A new approach exploring the uncertainties of climate sensitivity. *Atmos. Sci. Lett.,* **15,** 97–102, doi:10.1002/asl2.472.

Soden, B. J., I. M. Held, R. Colman, K. M. Shell, J. T. Kiehl, and C. A. Shields, 2008: Quantifying climate feedbacks using radiative kernels. *J. Climate,* **21,** 3504–3520, doi:10.1175/2007JCLI2110.1.

Steele, M., R. Morley, and W. Ermold, 2001: PHC: A global ocean hydrography with a high-quality Arctic Ocean. *J. Climate,* **14,** 2079–2087, doi:10.1175/1520-0442(2001)014<2079:PAGOHW>2.0.CO;2.

Stein, U., and P. Alpert, 1993: Factor separation in numerical simulations. *J. Atmos. Sci.,* **50,** 2107–2115, doi:10.1175/1520-0469(1993)050<2107:FSINS>2.0.CO;2.

Taylor, K. E., R. J. Stouffer, and G. A. Meehl, 2012: An overview of CMIP5 and the experiment design. *Bull. Amer. Meteor. Soc.,* **93,** 485–498, doi:10.1175/BAMS-D-11-00094.1.

Taylor, P. C., R. G. Ellingson, and M. Cai, 2011a: Geographical distribution of climate feedbacks in the NCAR CCSM3.0. *J. Climate,* **24,** 2737–2753, doi:10.1175/2010JCLI3788.1.

——, ——, and ——, 2011b: Seasonal variations of climate feedbacks in the NCAR CCSM3. *J. Climate,* **24,** 3433–3444, doi:10.1175/2011JCLI3862.1.

——, M. Cai, A. Hu, J. Meehl, W. Washington, and G. J. Zhang, 2013: A decomposition of feedback contributions to polar warming amplification. *J. Climate,* **26,** 7023–7043, doi:10.1175/JCLI-D-12-00696.1.

Vavrus, S., 2004: The impact of cloud feedbacks on Arctic climate under greenhouse forcing. *J. Climate,* **17,** 603–615, doi:10.1175/1520-0442(2004)017<0603:TIOCFO>2.0.CO;2.

Vial, J., J.-L. Dufresne, and S. Bony, 2013: On the interpretation of inter-model spread in CMIP5 climate sensitivity estimates. *Climate Dyn.,* **41,** 3339–3362, doi:10.1007/s00382-013-1725-9.

Watanabe, M., and Coauthors, 2010: Improved climate simulation by MIROC5: Mean states, variability, and climate sensitivity. *J. Climate,* **23,** 6312–6335, doi:10.1175/2010JCLI3679.1.

——, and Coauthors, 2012: Using a multiphysics ensemble for exploring diversity in cloud–shortwave feedback in GCMs. *J. Climate,* **25,** 5416–5431, doi:10.1175/JCLI-D-11-00564.1.

Wu, D. L., and J. N. Lee, 2012: Arctic low cloud changes as observed by MISR and CALIOP: Implication for the enhanced autumnal warming and sea ice loss. *J. Geophys. Res.,* **117,** D07107, doi:10.1029/2011JD017050.

Yoshimori, M., T. Yokohata, and A. Abe-Ouchi, 2009: A comparison of climate feedback strength between CO_2 doubling and LGM experiments. *J. Climate,* **22,** 3374–3395, doi:10.1175/2009JCLI2801.1.

——, M. Watanabe, A. Abe-Ouchi, H. Shiogama, and T. Ogura, 2014: Relative contribution of feedback processes to Arctic amplification of temperature change in MIROC GCM. *Climate Dyn.,* **42,** 1613–1630, doi:10.1007/s00382-013-1875-9.